LAWRENCE
LIVERMORE
NATIONAL
LABORATORY

LLNL-JRNL-641712

Evaluation of nanolipoprotein particles (NLPs) as an in vivo delivery platform

N. O. Fischer, D. Weilhammer, C. Thomas, M. Hwang, M. Corzett, C. Lychak, S. Urbin, N. Collette, J. C. Chang, G. Loots, A. Rasley, C. D. Blanchette

August 1, 2013

PLOS One

Disclaimer

Evaluation of nanolipoprotein particles (NLPs) as an in vivo delivery platform

Nicholas O. Fischer[1], Dina R. Weilhammer[1], Cynthia Thomas[1], Mona Hwang[1], Michele Corzett[1], Cheri Lychak[1], Salustra Urbin[1], Nicole Collette[1], Jiun Chiun Chang[2], Gabriela G. Loots[1,2], Amy Rasley[1*] and Craig D. Blanchette[1,*]

1 Biosciences and Biotechnology Division, Lawrence Livermore National Laboratories, Livermore, CA, 94551
2 University of California at Merced, School of Natural Sciences, Merced, CA, USA

***** Author to whom correspondence should be addressed
E-Mail: blanchette2@llnl.gov; Tel.: +925-422-5706; Fax: +925-422-2282
E-Mail: rasley2@llnl.gov; Tel: +925-423-1284; Fax: +925-422-2282

Abstract

Nanoparticles hold great promise for the delivery of therapeutics, yet limitations remain with regards to the use of these nanosystems for efficient long-lasting targeted delivery of therapeutics, including imparting functionality to the platform, in vivo stability, drug entrapment efficiency and toxicity. To begin to address these limitations, we evaluated the functionality, stability, cytotoxicity, toxicity, immunogenicity and in vivo biodistribution of nanolipoprotein particles (NLPs), which are mimetics of naturally occurring high density lipoproteins (HDLs). We found that a wide range of molecules could be reliably conjugated to the NLP, including proteins, single-stranded DNA, and small molecules. The NLP was also found to be relatively stable in complex biological fluids and displayed no cytotoxicity in vitro at doses as high as 320μg/ml. In addition, we observed that *in vivo* administration of the NLP daily for 14 consecutive days did not induce significant weight loss or result in lesions on excised organs. Furthermore, the NLPs did not display overt immunogenicity with respect to antibody generation. Finally, the biodistribution of the NLP *in vivo* was found to be highly dependent on the route of administration, where intranasal administration resulted in prolonged retention in the lung tissue. The combined results of this study indicate that the NLP platform may be ideally suited for use as both a targeted and non-targeted in vivo delivery vehicle for a range of therapeutics.

Introduction

The advent of nanotechnology has resulted in a variety of new possibilities for targeted delivery of therapeutic agents. In particular, delivery of therapeutic agents facilitated by nanoparticles is being implemented to solve several limitations of conventional drug delivery systems, including nonspecific bio-distribution and targeting, poor aqueous solubility, limited oral bioavailability, and low therapeutic indices [1]. Several types of nanoparticles have been developed to achieve targeted delivery of therapeutics, including inorganic nanoparticles [2], polymeric-based nanoparticles [3], polymeric micelles [4], dendrimers [5], liposomes [6], viral nanoparticles [7] and carbon nanotubes [8], each offering unique characteristics in nanoparticle composition, structure, and method of assembly. Despite the significant advantages these delivery vehicles provide over conventional drug delivery systems, there are still limitations with regards to the use of these nanosystems for efficient long-lasting targeted delivery of therapeutics, including *in vivo* stability, immunogenicity, targeting specificity, drug entrapment efficiency, long term storage, and toxicity [9]. One approach to address the issues associated with current nanoparticle platforms, particularly immunogenicity and toxicity, is to utilize a nanoconstruct that mimics supramolecular structures naturally present in the human body. One notable example of such a system is the lipoprotein class of nanoparticles, or high density

lipoproteins (HDLs), which are naturally present in most metazoan species and play an essential role in mammalian control of lipid metabolism [10]. These endogenous nanoparticles are utilized to transport hydrophobic cholesterol and triglycerides to cells through the circulatory system. The structure and function of HDLs *in vivo* have been studied for the past three decades and methods for assembling several different compositionally distinct HDLs *ex vivo* [also called reconstituted HDLs (rHDLs), nanodiscs, or nanolipoprotein particles (NLPs)] have been developed [11-14]. The vast majority of the work on rHDLs and NLPs has been directed at both understanding the biology of such particles [15-18] as well as exploring their utility in solubilizing and stabilizing membrane proteins in discrete, native lipid environments [19-24]. However, the use of these particles for delivery of therapeutic drugs [25-28], diagnostic imaging [29], and vaccine applications [30-32] has only recently been examined.

NLPs are nano-scale (8-25 nm) discoidal membrane bilayer mimetics that form through spontaneous self-assembly of purified lipoproteins and lipids [11-13]. NLP formation and self-assembly is initiated by incubating detergent-solubilized lipids with apolipoproteins. Upon the removal of detergent, the lipid molecules assemble into nanoscale lipid bilayers that are stabilized at their periphery by lipoproteins. The amphipathic lipoproteins are oriented such that the lipophilic face interacts with the alkyl chains of the lipid bilayer, whereas the polar face is solvent-exposed. While the assembly of NLPs is facile, the diversity in both the lipid and protein [12,33] constituents illustrates the robust nature of the assembly process. In addition, due to the inherent amphipathic nature of lipid bilayers, the NLP platform is amenable to the incorporation of diverse lipids (in terms of both fatty acid chains and polar headgroups) and other hydrophobic or amphipathic molecules (e.g. cholesterol). The relative ease of forming NLPs through self-assembly, the ability to incorporate myriad lipophilic molecules within the NLP bilayer, and the diverse tool-kit of functionalized lipids either commercially available or readily synthesized suggest that NLPs are highly amenable to accommodate a disparate range of cargo molecules. Importantly, since these particles are naturally present in the human body, the NLP platform is less likely to result in issues facing other nanoparticle systems that are currently used for the targeted delivery of therapeutics, such as immunogenicity, stability in complex biological fluids, and toxicity.

Thus, to assess the potential of using NLPs as an *in vivo* platform for the delivery of therapeutics, we examined 1) the potential of conjugating multiple, different molecules of disparate physicochemical properties to the NLPs, 2) the stability of the NLP in complex biological fluids, 3) the cytotoxicity of the NLP platform in relevant cell types, and 4) the *in vivo* bio-distribution of the NLPs administered by four different routes. The combined results of this work indicate that this platform is ideally suited for both targeted and non-targeted delivery of therapeutic agents, and has broad biomedical applications.

Materials and Methods

Materials: 1,2-dioleoyl-*sn*-glycero-3-phosphocholine (DOPC), 1,2-dimyristoyl-*sn*-glycero-3-phosphocholine (DMPC), 1,2-dioleoyl-*sn*-glycero-3-((N(5-amino-1-carboxypentyl)iminodiacetic acid) succinyl)(nickel salt) (Ni-lipid), and 1,2-distearoyl-*sn*-glycero-3-phosphoethanolamine-N-[folate(polyethylene glycol)-2000] (ammonium salt) (DSPE-PEG2000-folate) (PF) were purchased from Avanti Polar Lipids (Alabaster, AL). All other reagents were ordered from Sigma-Aldrich (St. Louis, MO). NHS-PEG4-DBCO was purchased from Click Chemistry Tools (Scottsdale, AZ). The cholesterol-modified oligodeoxynucleotide (cODN) (5'–TCAACATCAGTCTGATAAGCTA–tetraethyleneglycol–cholesterol–3') was purchased from Integrated DNA Technologies (Coralville, IA). The C18-PEG6-N_3 molecule was custom synthesized by Creative PEGworks (Winston Salem, NC). RPMI1640, Opti-MEM fetal bovine serum, NHS-activated Alexa Fluor 647 (AF647), NHS-activated Alexa Fluor 750 (AF750), primary antibodies and secondary antibodies were obtained from Invitrogen (Carlsbad, CA). ELISA kits for cytokine analysis were purchased from R&D systems (Minneapolis, MN). The kits for LDH and MTT analysis were purchased from Promega (Madison, WI) and Invitrogen.

Protein expression and purification: The expression clone for the 22 kDa N-terminal fragment of human apolipoprotein E4 (apoE422k, kindly provided by Dr. Karl Weisgraber) featuring a cleavable His-tag [34] was expressed and purified as previously described [11,35]. The expression clone for the *Y. pestis* protein used in this study, LcrV, was expressed and purified as previously described [31].

For expression of FTN_0841 (0841), the full length FTN_0841 ORF was amplified from genomic DNA isolated from *F. tularensis* subsp. *novicida* strain U112 using gene specific primers (forward primer: 5' - ctcgaattcCATATGAAAAATGTCTTAATGGTTACC, reverse primer 5' - ggaattGGATCCATTAAATAGTGATTGTTTTATTGCTT) containing engineered 5' NdeI and 3' BamHI endonuclease sites. The PCR amplified 0841 gene was cloned into a modified pETBlue expression plasmid, pETBlueER by directed cloning. The resulting plasmid encoded a native 0841 protein appended with a C-terminal His-tag (GSLEHHHHHH). Expression plasmids encoding 0841 were propagated in *E. coli* DH5α-Ti cells and colonies carrying the plasmid were selected on LB/agar plates with 100 μg/ml ampicillin. Plasmid DNA was then transformed into BL21(DE3)pLacI competent cells (Novagen) for expression. Individual colonies were grown in LB media containing 100 μg/ml ampicillin at 37° to O.D. 600 of ~0.6 and protein expression was induced by the addition of isopropyl thiogalactoside (IPTG) at a final concentration of 1 mM for 3 hrs. The bacteria were pelleted by centrifugation at 4000 x g and frozen. The thawed bacterial pellet was resuspended in 50 mM

sodium phosphate, 300 mM sodium chloride, 10 mM imidazole, pH 8.0 and lysed for 20 min in a high pressure homogenizer (Emulsiflex-C5, Avestin). Lysates were centrifuged at 8,000 x g to remove insoluble material. 0841 was initially purified from the clarified supernatant by nickel affinity chromatography using a 5 ml HisTrap FF Column (GE Healthcare) on an AKTA FPLC (GE Healthcare). The column was washed with 50 mM NaH_2PO_4, 300mM NaCl, 20mM Imidazole pH 8 and the His tagged protein was eluted with 50 mM NaH_2PO_4, 300mM NaCl and 250mM imidazole pH 8.0. The eluted protein was further purified and buffer exchanged into 10 mM Hepes, 50 mM NaCl pH 7.5 on a Superdex 75 HiLoad 26/60 column (GE Healthcare). Fractions containing protein were analyzed by SDS-PAGE stained with SYPRO Ruby (Invitrogen) to assess purity and concentrated using Vivaspin 20 5000 kDa MWCO (Sartorius) to a final concentration of 11 mg/ml.

NLP assemblies: NLPs were assembled according to a previously reported procedure [11,35] with slight modifications. Briefly, lipids were either prepared or obtained in chloroform and aliquoted into glass vials. The total lipid-to-apoE422k molar ratio was 80:1. Chloroform was then removed using a stream of N_2 under agitation to form a thin lipid film. Lipids were then solubilized in PBS buffer (137 mM sodium chloride, 2.7 mM potassium chloride, 10 mM phosphate buffer, pH 7.4) using 30 mM sodium cholate. After addition of the apoE422k (150 μM in final assembly volume), samples were incubated at 23.8°C for at least 2 hours. Assemblies were dialyzed overnight against PBS to remove cholate. Samples were subsequently analyzed and purified by SEC (Superdex 200, 10/300 GL column, GE Healthcare, Piscataway, NJ) in PBS buffer (0.5 mL/min flow rate). The exclusion limit of the column was determined with Blue Dextran 2000. SEC fractions (250 μl) were collected every 30s. SEC fractions containing homogeneous NLP populations were concentrated using 50k molecular weight cut-off (MWCO) spin concentrators (Agilent Technologies, Santa Clara, CA). The apoE422k concentration was determined using the Advanced Protein Assay Reagent (Cytoskeleton Inc., Denver, CO), where BSA was used as the standard. The concentrated NLP samples were then stored at 4°C until further use.

Labeling the NLPs with Alexa dyes: NLPs were labeled with either AF647 (stability experiments) or AF750 (biodistribution experiments) by incubating the NLPs with the respective reactive dye for at least 2 hrs (5:1 dye:NLP molar ratio). The reaction was performed in PBS buffer containing 5 mM sodium bicarbonate, pH 8.2. After completion of the reaction, 10 mM Tris pH 8.0 was added to quench any unreacted dye and incubated for 30 minutes. The samples were then run on SEC (Superdex 200 PC 3.2/30 column, GE Healthcare, Piscataway, NJ) to purify out the labeled NLP from unreacted dye (0.15 mL/min flow rate). The SEC fractions corresponding to the NLP were then pooled and

concentrated using 50 kDa MWCO spin concentrators. The apoE422k concentration was determined using the Advanced Protein Assay Reagent (Cytoskeleton Inc., Denver, CO), where BSA was used as the standard. The concentrated NLP samples were then stored at 4°C until further use.

Analysis of conjugation of biological molecules to the NLP: Due to the significant size difference between the NLPs and free protein, SEC was used as a quantitative tool to assess conjugation of biological molecules to the NLP. NLP samples were analyzed by SEC (Superdex 200 PC 3.2/30 column, GE Healthcare) in PBS buffer. A flow rate of 0.15 ml/min was used to ensure no overlap in the elution of unbound protein and NLP. The samples were monitored and detected at an absorbance wavelength of 280 nm. For analysis and purification of covalent protein attachment to the NLPs, the Superdex 200, 10/300 GL column (GE Healthcare) was used at a flow rate of 0.5 ml/min. For the protein conjugation experiments, purified NLP fractions were analyzed by SDS-PAGE, using SYPRO Ruby protein gel stain for visualization. Densitometry was used to quantify conjugated protein, using appropriate 0841 protein standards. Previously, computational modeling of apoE422k containing NLPs indicated that NLPs 23.5 nm in diameter have 6 apoE422k per NLP. Therefore, in these experiments, the NLP concentration was calculated based on the E422k concentration by assuming that each NLP contained 6 apoE422k scaffold proteins [11,36].

SEC analysis of NLP stability in complex biological fluids:
AF647-labeled NLPs were purified to homogeneity with diameters averaging 23.5 nm [36]. NLP samples were incubated in increasing serum concentrations and subsequently analyzed by SEC (Superdex 200 PC 3.2/30 column, GE Healthcare) in PBS buffer. A flow rate of 0.15 ml/min was used to ensure no overlap in the elution of disassembled apoE422k and intact NLP. The NLPs labeled with AF647 were monitored at an absorbance wavelength of 600 nm to avoid interfering signals at 280 nm from serum proteins and constituents. NLP peak integration was used to assess NLP disassembly as a function of incubation time using instrument software (LC Solutions, Shimadzu). These experiments were performed with NLPs made with 35% Ni-lipid and either 65% DOPC or 65% DMPC.

Isolation of primary splenic immune cells: Spleens were harvested from male BALB/c mice (4-6 weeks old) and single cell suspensions of splenoctyes were generated as follows. Briefly, spleens were injected with 200-500 µl of a solution of liberase (1.67 U/ml, Roche) and DNAse I (0.2 mg/ml, Roche) in RPMI + 10% FBS and incubated for 30 minutes at 37°C before manual dissociation through 70 µm filters. Red blood cells were lysed by incubation in 1 ml ACK lysis buffer (Life technologies) for 5 minutes at room temperature. The single cell suspension of splenocytes was then sorted by positive

selection into CD11c+ (dendritic cell), $CD5^+$ (T cell), $CD19^+$ (B cell), $CD49b^+$ (NK cell) and $CD11b^+$ (macrophage) populations using MACS bead sorting according to manufacturer's instructions (Miltenyi Biotech). All experiments were conducted after review and approval by the Institutional Animal Care and Use Committee at Lawrence Livermore National Laboratories.

Cytotoxicity measurements: The cytotoxicity of the NLP platform in J774A.1 (J774, mouse macrophage cell line) and primary peritoneal macrophages (pMPs) were measured using a LDH-based viability assay, whereas the cytotoxicity of the NLP against UMR (mouse osteoblastic cell line) cells was measured using the MTT-based viability assay. For the J774 and pMPs cytotoxicity experiments, $0.5 \text{ X } 10^6$ cells were plated into 24 well plates in 0.5 ml of Opti-MEM media (Invitrogen). After incubation with varying concentrations of NLPs for 24 hours, LDH levels were measured using the CytoTox96 non-radioactive cytotoxicity assay from Promega (Madison, WI) following manufacturer's instructions. Briefly, 50 µl of the cell supernatant was added to 50 µl of LDH substrate and incubated for 30 minutes. After this incubation period, 50 µl of the stop solution was added and the sample absorbance was measured at a wavelength of 490 nm. The data was normalized to cells that were subjected to multiple freeze-thaw cycles. For the UMR cytotoxicity experiment, $1 \text{ X } 10^4$ cells were seeded into 96 well plates in 200 µl Opti-MEM media. The cells were then incubated with different NLP concentrations for 24 hrs. The media was then replaced with 150 µl of fully supplemented F-12 MEM and incubated for 4 hr. The wells were then washed with fresh F-12 MEM media and 10 µl of a 12 mM stock solution of MTT was added. The plates were then incubated at 37ºC for 4 hours. 100 µl of an SDS-HCL solution (0.1 M SDS) was added to each well and mixed thoroughly with a pipette. The plates were then incubated at 37ºC overnight in a humidified incubator and the absorbance at 570 nm of each well was measured. All cytotoxicity experiments were performed with NLPs consisting of 35% Ni-Lipid and 65% DOPC.

In vivo acute toxicity: To evaluate the acute toxicity of the NLP, groups of 6 five week old BALB/c mice (3 males and 3 females) were administered the NLP via the intraperitoneal (i.p.) or intranasal (i.n.) route daily for 14 days. The daily NLP dose was 25 µg (based on E422k protein) and inocula for i.p. and i.n. administration were delivered in a total volume of 100 µl and 30 µl, respectively, in PBS. The weights of the mice were recorded daily each morning. After the 14 day period, the mice were euthanized and liver, kidney, lung and spleen were harvested. The weight of each organ was recorded and normalized to the weight of the mouse, which was recorded just prior to euthanization. All acute toxicity experiments were performed with NLPs consisting of 35% Ni-Lipid and 65% DOPC. All

experiments were conducted after review and approval by the Institutional Animal Care and Use Committee at Lawrence Livermore National Laboratories.

Immunogenicity of the NLP platform: To determine the immunogenicity of the NLP platform, groups of 10 BALB/c mice (5 males and 5 females) were immunized with the NLP (25 µg) and LcrV (10 µg)+CpG (5 µg) (positive control) via the i.p. and i.n. routes. Inocula for i.p. and i.n. administration were delivered in a total volume of 100 µl and 30 µl, respectively, in PBS. Serum was then collected from the mice 3 weeks post-immunization via the saphenous vein. The collected sera were than pooled from each animal in a given experimental group and subjected to ELISA analysis as described previously [37]. For the ELISA analysis, Immulon 2HB microtiter plates (Thermo Labsystems, Franklin, MA) were coated with the appropriate antigen (LcrV or apoE422k) (200 ng/well), and then incubated with sera at increasing dilutions for 1 hour. Goat anti-mouse IgG HRP-conjugated antibody (KPL Inc., Gaithersburg, MD) was added to the plates for 1 hour, and the bound HRP was detected by incubation with TMB (Sigma), quenched after 5 min with 1 M HCl. The reaction product was measured spectrophotometrically at 450 nm, and values were corrected for background activity detected from wells that received diluent in place of sera. The titration curves were then fit to a power function in MS Office Excel 2010 and titers were calculated from the fit function using a cutoff absorbance value of the average background O.D. + 3 S.D. All experiments were conducted after review and approval by the Institutional Animal Care and Use Committee at Lawrence Livermore National Laboratories.

Biodistribution of the NLP platform: To measure the biodistribution of the NLP, NLPs were first labeled with AF750 as described above. Groups of three mice were then immunized with 50 µg of NLP via i.p., intramuscular (i.m.), subcutaneous (s.c.) and i.n. administration. After predetermined time points, the mice were euthanized and spleen, kidney, liver and lungs removed. The fluorescence intensities in the excised organs were analyzed using a Kodak image station 4000R digital imaging system (Rochester, NY) at an excitation and emission wavelength of 750 +/- 20 nm and 790 +/- 20 nm. The fluorescence values of each organ were then normalized to the organ weight after subtracting for background fluorescence. All experiments involving animals were conducted after review and approval by the Institutional Animal Care and Use Committee at Lawrence Livermore National Laboratories.

Results and Discussion

Multifunctional NLPs

Any nanoscale platform that is to be utilized as a universal vehicle for the delivery of therapeutics must be amenable to conjugation or incorporation of a diverse range of molecules featuring unique physical and chemical properties. For example, therapeutic cargo molecules can range in size, solubility, charge, and available reactive groups. Functionalizing the nanoparticle surface with reactive chemical moieties is a strategy commonly employed to achieve conjugation of therapeutic molecules, and has been used extensively with great success. However, for many of these nanoparticle systems attaining functional activity on the surface of the particle is not trivial and often requires significant modifications to the particle constituents and synthesis protocols or costly additional steps post-synthesis, such as grafting the surface with a functionalized polymer [38-40]. Thus, most particulate systems are engineered to readily incorporate molecules of similar physical or chemical properties, rather than a host of biological molecules with highly disparate properties. However, these issues can be readily mitigated when utilizing the NLP platform because the lipid bilayer is so versatile in accommodating myriad amphipathic and lipophilic molecules. We have essentially developed two facile and generally applicable methods for conjugating biomolecules to the NLP platform. First, NLPs can be assembled with functional lipids (lipids bearing a functional head group) for conjugation of molecules featuring the corresponding chemical reactivity (Figure 1A), illustrated by both covalent and non-covalent coupling chemistries. Second, cargo molecules containing lipophilic groups (e.g. cholesterol) that are either native to the molecule or chemically appended can be tethered to the NLP, whereby the lipophilic group anchors the compound to the NLP lipid bilayer (Figure 1B). This approach was demonstrated by incorporating cholesterol-modified oligonucleotides and the small molecule folate conjugated to a pegylated lipid to the NLP lipid bilayer. Importantly, these two broadly applicable methods can be used orthogonally to conjugate multiple biological molecules of disparate chemistries to the NLP (Figure 1C).

To demonstrate the ease of conjugating biomolecules to a functionalized NLP lipid bilayer, strategies for both covalent and non-covalent conjugation of recombinant proteins were assessed. Each approach involved the formation of a multi-component lipid bilayer, utilizing a chemically functionalized lipid in conjunction with a bilayer-forming, non-reactive phospholipid. For non-covalent protein attachment, the non-covalent interaction between chelated nickel atoms and polyhistidine-tagged proteins, which has been extensively employed in both protein purification and conjugation strategies, was used. To enable conjugation of His-tagged proteins to the NLP, a commercially available nickel-chelating lipid (NiLipid) was incorporated into the NLP bilayer. We have previously demonstrated that NLP compositions with NiLipid constituting 35% of total bilayer lipid provides the greatest conjugation efficiency in our system [36]. The purified NiNLPs were incubated with a His-tagged protein (0841

from *Francisella tularensis*) for 30 minutes and analyzed by size exclusion chromatography, an analytical method well suited for the characterization of biomolecule conjugation to functionalized NLPs [12,13,33,36]. Free proteins typically have a retention time (t_R) between 11.5 and 12.5 min, compared to a t_R ~7.8 min for the larger NLP; thus, if no protein is attached to the NLP, a free peak should be observed at t_R between 11.5 and 12.5 min. The black line in Figure 2A corresponds to the NiNLP in the absence of the His-tagged protein. As expected the t_R of the NiNLP alone was ~7.8 min. When His-tagged 0841 was incubated with the NiNLP at increasing 0841:NiNLP ratios prior to SEC analysis, the NLP t_R decreases with a concomitant increase in signal intensity (both indicators of successful cargo attachment) (Figure 2A). In addition, no free protein peak was observed at 0841:NiNLP ratios below 40:1 (Figure 2A). These combined observations indicate that the His-tagged 0841 protein was successfully conjugated to the NLP platform. To verify attachment, SEC fractions corresponding to the 0841:NiNLP complex were analyzed by SDS-PAGE. As shown in Figure 2B (inset), both 0841 and apoE422k were co-localized in the NLP fractions, and 0841 band intensity increased commensurate with increasing ratios of 0841 to NLP. Densitometry of the SDS-PAGE gel bands was used to quantify the amount of 0841 immobilized on the NLPs at increasing concentrations, and expressed as a function of the initial reaction ratio in Figure 2B. Importantly, this relationship was almost linear with a slope of 0.91 up to a ratio of 20:1. These results indicate that below ratios of 20 0841 molecules per NLP, near complete conjugation of the His-tagged protein was achieved. These combined results demonstrate that the His-tagged 0841 protein was successfully conjugated to the NiNLP platform. We have also demonstrated successful conjugation of over 20 different His-tagged proteins to the NiNLP platform [30,33,36].

Although the outlined non-covalent conjugation strategy was facile and highly efficient, the binding is reversible. As previously reported, the off-rates of His-tagged proteins from NiNLPs can range between 5 hours and 10 minutes [36], which may not be a sufficiently long retention time for many applications; thus, a covalent conjugation strategy was employed. An important consideration for specific and tailored covalent conjugation of a biomolecule to the NLP is to ensure that chemoselective reaction pairs are used, specifically avoiding at a minimum biological functional groups present on the E422k scaffold protein (e.g. amino and carboxyl groups). To address this issue, azide-alkyne cycloaddition reactions (click chemistry) were investigated. Specifically, we took advantage of recent publications demonstrating strain-promoted alkyne-azide cycloaddition reactions (SPAAC) that do not require either copper catalysts or organic solvents to be effective [41-44]. NLPs were assembled with alkyl-modified azide moiety (C18-PEG6-N_3), which was readily incorporated during the self-assembly reaction to form N_3NLPs. To achieve conjugation of a protein through click chemistry, the 0841 protein was first modified to contain an alkyne moiety by covalently coupling the NHS-activated

strained alkyne molecule dibenzylcyclooctyne (DBCO) to free amines on the 0841 surface. After purifying the DBCO-functionalized 0841 (0841-DBCO), the 0841-DBCO was incubated with the N_3NLP for 24 hrs at 4°C and analyzed by SEC (Figure 2C). The black trace in Figure 2C corresponded to the N_3NLP alone and the remaining lines corresponded to N_3NLPs incubated with the DBCO-protein for 24 hours at increasing ratios of DBCO-0841 to N_3NLP. A clear shift in t_R was observed for the N_3NLP:0841-DBCO construct relative to the N_3NLP alone, indicating successful conjugation. However, at all ratios tested, a significant peak corresponding to free 0841 was observed, indicating that the reaction was not 100% efficient. It is worth noting that because of the significant amount of unreacted protein, a larger diameter SEC column for separation providing greater resolution was required, which is the reason for the difference in t_R between Figure 2A and 2C. To further verify that covalent attachment was successful, the peaks corresponding to the N_3NLP:0841-DBCO construct were analyzed by SDS-PAGE and quantified by densitometry. As shown in Figure 2D (inset), both E422k and 0841-DBCO were present in the NLP SEC fractions. These results demonstrate that the DBCO-protein was successfully conjugated to the NiNLP platform. When final conjugate ratios were expressed as a function of the initial reaction ratio (Figure 2D), a linear relationship was observed up to 20 proteins per NLP, with a significantly smaller slope compared to the non-covalent approach (0.53 vs. 0.91). Based on these experimental data, significant protein remains unreacted with the N_3NLP, which is widely reported with these types of strained cycloaddition reactions. Comprehensively, these results demonstrate our ability to successfully covalently attach a protein to the NLP platform using click chemistry, although the coupling reaction is less efficient than the comparable non-covalent approach.

In addition to utilizing functionalized lipids for subsequent attachment of biological molecules with the corresponding chemistry, we have also developed methods to attach molecules that have been appended with a lipophilic compound (Figure 3). The first compound tested was a cholesterol-modified oligodeoxynucleotide (cODN). This ssDNA molecule is complementary to the micro RNA mir21, an anticancer therapeutic target [45]. NLPs were assembled at different cODN:NLP ratios and analyzed by SEC (Figure 3A). Mirroring the results seen with conjugating protein molecules to the NLPs, a decrease in t_R of the cODN:NLP was paired with significant increases in peak absorbance intensity. The post-purification cODN:NLP ratios were quantitatively measured based on intrinsic absorbance, as described in the materials and methods. As illustrated in Figure 3B, the incorporation of the cODN was very efficient and followed a linear trend in the range tested (up to cODN:NLP ratio of 40:1) (slope = 1.04).

To further demonstrate the feasibility of using this approach to attach biological molecules to the NLP platform, NLPs were assembled with DPSE-PEG2000-folate (PF) at increasing ratios (Figure 3C). As

was observed for the cODN:NLP, there was a clear shift to a shorter t_R and an increase in the peak intensity when the NLPs were assembled with the PF (7.6 min vs. 7.8 min), both of which indicate successful conjugation. In addition, no free PEG-folate peak was observed, which indicates that all of the PEG-folate added during assembly was incorporated into the NLP platform. The actual PF:NLP ratios were analyzed by UV-Vis as described in the materials and methods section and again a near linear relationship (slope = 0.71) was observed when the post-assembly PF:NLP was plotted as a function of the input PF:NLP (Figure 3D). Based on these combined results, the NLP platform is ideally suited for attachment of a wide range of molecules with disparate chemical and functional properties, which is an important attribute of any nanoparticle system that is to be used for the in vivo delivery of therapeutic agents.

NLP stability in complex biological fluids

A key attribute necessary for any nanoparticle-based delivery vehicle is long term stability in complex biological fluids. Some of the drawbacks associated with current nanoparticle technologies include lack of stability in complex biological fluids [46,47] or loss of function do to non-specific adsorption of serum proteins onto the particle surface (e.g. biomolecule corona) [48,49]. Therefore, SEC was used to evaluate the stability and non-specific protein coating of the NLP platform in media (RPMI 1640) containing serum levels ranging from 20 to 100% (spanning relevant *in vitro* and *in vivo* conditions) (Figure 4). To facilitate monitoring of NLP size and integrity by SEC, NLPs were labeled with AF647 to provide a spectrophotometric signature unperturbed by intrinsic absorbance of serum proteins and constituents. The t_R of the intact NLP was distinct from free E422k released from dissociated NLPs (9 min vs. 12 min, respectively), and thus the stability and integrity of the NLP could be readily followed over time by SEC. Two different types of NLPs were assembled to interrogate the effect of NLP lipid composition on NLP stability; one consisting of DMPC (fully saturated lipid – DMPC:NLP) and the other DOPC (mono-unsaturated lipid – DOPC:NLP). We also examined the effect of temperature on NLP stability (25ºC vs. 37ºC). Figure 4 shows the SEC chromatograms of DMPC:NLPs incubated in 20% sera for 0, 4, 8 and 24 hr at 25ºC. At 0 hr, only a single peak, corresponding to intact NLP (t_R ~7.8 min) was observed. At longer incubation times, dissociated E422k (t_R 12 min) was observed concomitant with a decrease in the intensity of the intact NLP peak, indicating a gradual dissociation of the NLP. These chromatograms were used to quantify the rate of NLP dissociation by integrating the NLP peak area. Figure 5A and 5B show the dissociation of the DOPC:NLPs and DMPC:NLPs, respectively, at 25ºC as a function of the different sera concentrations. As can be observed from these traces, the DMPC:NLPs were considerably less stable as a function of time than the DOPC:NLPs. To quantify this difference, the integrated areas of the NLP and E422k peaks in Figure 5A and 5B were fit

to an exponential decay function and the half-life of the particle ($t_{1/2}$) under each condition was calculated (Figure 5C). Based on these analyses, we discerned a measurable decrease in the NLP stability at increasing sera concentrations, whereby the DMPC:NLPs were significantly less stable than the DOPC:NLPs at all sera concentrations tested. At 25°C, the maximum $t_{1/2}$ of the DOPC:NLPs was 128.8 hrs (20% sera), whereas the maximum $t_{1/2}$ of the DMPC:NLPs was 8.3 hrs (20% sera) To examine the stability of these particles under more biologically relevant conditions, these experiments were repeated at 37ºC (Figure 5D-5F). Overall, the DMPC:NLPs were considerably less stable than the DOPC:NLPs at all sera concentrations tested (Figure 5F). One possible reason for the difference in NLP stability between these two particles may be due to lipid-lipid and lipid-scaffold interactions. Although the structure of the NLP has long been reported to be a static discoidal structure, more recent studies have indicated that the NLP structure is more dynamic in solution and may adopt multiple different conformations ranging from discoidal to spherical [50]. DOPC lipid bilayers are more loosely packed than DMPC bilayers due to the presence of the unsaturated double bond in the acyl chain of the lipid. Thus, this more loosely packed structure may allow for more flexibility in the three dimensional morphology of the NLP, i.e. allowing it to more readily adopt these different conformations relative to the more packed structure of DMPC based NLPs, which may explain this increase in stability of the DOPC-based NLPs. However, further studies would be needed to conclusively determine the reasons for this increased stability.

It is also worth noting that regardless of the serum concentration, no significant shift in the NLP t_R was observed, suggesting that an increase in particle size due to non-specific serum protein adsorption or protein corona formation did not occur. While the peak t_R did slightly decrease with time under each serum condition (~7.8 min to ~ 6.8 min), this decrease was relatively small and was likely caused by a rearrangement in NLP size due to the loss of total E422k associated with the particles during degradation, as has been documented with similar NLP constructs [51]. These data suggest that NLPs avoid significant non-specific interactions with serum protein, a challenge faced by many other nanoparticles platforms, including inorganic nanoparticles [21].

In vitro cytotoxicity

Cytotoxicity has been documented for metal based nanoparticles [52,53] and other non-biological based nanoparticles, such as dendrimers [54]. These types of nanoparticle platforms often require complex modifications to limit their cytotoxic effects. In contrast, the NLP platform consists solely of biocompatible components and is in fact a mimic of nanoparticles that are present in the human body (HDLs); thus, we hypothesized that the cytotoxic effect of NLPs would be minimal. The cytotoxicity of the NLP platform was evaluated using UMR-106 (rat osteosarcoma), J774 (mouse macrophage cell

line) cells, pMPs, primary mouse dendritic cells (pDCs), primary mouse natural killer (pNK) cells, primary mouse B cells (pBC), primary mouse T cells (pTC) and HEP-G2 (human hepatic carcinoma) cells. The NLPs displayed no cytotoxic effects when incubated with the UMR-106 cells at concentrations ranging from 1.6 – 50 μg/ml (based on amount of E422k in the sample; data was normalized to the PBS control) as assessed using the MTT assay (Figure 6A). Similarly, no toxicity was observed in J774 cells when incubated with NLPs at concentrations ranging from 0 – 52 μg/ml (based on amount of E422k in the sample; data was normalized relative to the PBS control and positive cells correspond to cells that were lysed by multiple freeze-thaw cycles) when determined using a lactate dehydrogenase (LDH) activity assay (Figure 6B). To further demonstrate the low cytotoxicity of the NLP platform, these experiments were repeated with a human liver cell line, Hep G2. This cell line has been widely used as a model cell line to assess potential cytotoxicity of drugs in the liver [55]. In these experiments, cells were incubated with 0, 5, 20, 40, 80 and 320 μg/ml of NLP for 24 hrs and cytotoxicity was measured using the LDH activity assay (Figure 6C). As observed with the other cell types, the NLPs displayed no significant cytotoxicity relative to the PBS control. Based on these initial results, we proceeded to evaluated the cytotoxicity of 25 μg/ml of NLP against a range of different primary mouse immune cells isolated from the spleen (macrophage cells, dendritic cells, natural killer cells, B cells and T cells) (Figure 6D). At this dose, no cytotoxicity was observed in any cell type examined. Thus, these combined data indicate that the NLP platform displays no cytotoxicity *in vitro*, even at concentrations as high as 320 μg/ml, which is likely due, in part, to the biocompatibility of the NLP composition.

In vivo acute toxicity

Next, we set out to determine whether NLPs were also non-toxic *in vivo*. Acute toxicity experiments were performed according to the National Toxicology Program published by the Department of Health and Human Services (http://ntp.niehs.nih.gov/). In these experiments, groups of six mice (3 male/ 3 female) were injected with 25 μg of NLP (based on E422k content) either through the i.p. or i.n. route daily for 14 consecutive days. The 25 μg dose was selected based on typical doses that have been previously used in NLP-based vaccine formulations [30,37]. Animals were weighed daily and assessed for overt signs of morbidity. As shown in Figure 7, no significant weight loss was observed in either males (Figure 7A) nor females (Figure 7B) over the course of 14 days relative to PBS control animals, indicating that daily administration of the NLP over this time period did not result in any overt signs of animal distress or diminished health. Similarly, no differences in responsiveness and activity level of the animals were observed between the groups. At the end of the 14 day time period, the mice were euthanized and liver, lung, kidney and spleen were collected, weighed, and visually inspected. No

obvious lesions were observed in any of the harvested tissues (data not shown) and no statistically significant differences were observed in normalized weights of the organs (organ weight/mouse weight) between the PBS group and the mice that received the NLP (Figure 8). These combined results demonstrate that the NLP platform was highly biocompatible and displayed no acute toxicity *in vivo* when administered daily over a two week period.

The low toxicity of the NLPs was not surprising given that the particles are essentially a mimetic of naturally occurring particles, HDLs. Therefore, we hypothesize that by utilizing a platform that mimics naturally occurring particles, we have significantly reduced any potential toxic effects that would be associated with the delivery vehicle itself. It is worth noting that HDLs are produced and processed in the liver, underscoring the possibility that this aggressive administration protocol could have caused adverse effects in this organ; however, this was not observed. Typical serum concentrations of HDLs in the mouse are approximately 0.45 mg/L [56], although this value can greatly fluctuate daily depending on diet. As such, the daily dose of 25 µg constituted only ~4% of total serum HDL levels (assuming an average blood volume of approximately 1.5 ml for a 25 g mouse and average HDL concentration of 0.45 mg/L), which is well within a tolerable HDL range.

In vivo immunogenic properties

One of the primary drawbacks of several nanoparticle based delivery vehicles is unintended immunogenic properties, which can cause unnecessary inflammatory side effects or result in rapid clearance of the particle by the immune system [57,58]. The origin of the immunogenicity of many of these particles is due to their foreign nature, i.e. the body recognizes the particle as non-self. However, because the NLP platform is a mimetic of naturally occurring HDLs, it is possible that it will be very weakly immunogenic. Therefore, the immunogenic properties of the NLP platform were evaluated *in vivo* by measuring antibody generation against the apoE422k scaffold protein. In these experiments, groups of 10 mice were immunized via i.p. and i.n. administration with the NLP. To provide a comparative sample known to elicit significant antibody titers, the *Y. pestis* antigen, LcrV, co-administered with the adjuvant CpG was used as a positive control. Four weeks post-immunization, apoE422k (NLP scaffold protein) (mice immunized with NLP) and LcrV specific IgG antibody titers (mice immunized with LcrV+CpG) were quantified by ELISA. Significant antibody generation was observed for the positive control, LcrV+CpG, whereas almost no antibody generation against the scaffold protein used to make the NLP was observed for either route of administration (Figure 9). It is worth noting that LcrV+CpG was chosen as a positive control because this is an established immunogenic formulation [31]. These results demonstrate that the platform in the absence of a cargo

molecule has non-significant immunogenic properties, which is an important attribute of any drug delivery vehicle.

In vivo biodistribution

Successful *in vivo* delivery of therapeutics using nanoparticle-based approaches requires sustained retention of the particles *in vivo* for maximal efficacy. To evaluate the biodistribution of the NLP construct *in vivo*, NLPs were labeled with AF750 and administered i.p., i.m., s.c. and i.n. The fluorescence intensities of dissected organs were quantified over time (2, 4, and 24 hrs) (Figure 10A-D) and normalized to total organ weight. Administration of fluorescent NLPs i.p. resulted in peak fluorescence intensities in the kidney, liver and spleen 2 - 4 hrs (Figure 10A) post-administration with most fluorescent signals diminished beyond 24 hrs post NLP administration. A similar trend was observed after i.m. and s.c. administration (Figure 10B-C), with the exception that the fluorescence intensity in the spleens were significantly lower when compared to i.p. administration. However, i.n. administration resulted in a much different biodistrubtion profile, where the majority of the signal was observed in the lung over the 24 hr time period, and to a lesser extent in the kidney (Figure 10D). These results imply that after i.n. administration the NLP platform is retained primarily in the lung and eventually processed by the kidney, which likely occurs through blood filtration. These results have important implications with regards to therapeutic delivery to the lungs. The lung environment has become an important target for the delivery of therapeutics using nanoparticle delivery vehicles due to the large alveolar surface area suitable for drug absorption, the low thickness of the epithelial barrier, extensive vascularization, relatively low proteolytic activity in the alveolar space when compared to other routes of administration, and the lack of first-pass metabolism [59-61]. In addition, it has also been reported that uptake of nanoparticles by alveolar macrophages is reduced with particle sizes below 260 nm [62]. The significantly higher retention observed in the lung compared to the other routes of administration suggests that this delivery route may be ideal for *in vivo* delivery of therapeutics using the NLP platform.

Because of the significant differences in the biodistribution profiles of i.n vs. i.p., i.m. or s.c., an in-depth time course analysis of NLP biodistribution was performed for the i.n. and i.p. routes (Figure 11). Mirroring the previous study, the fluorescence signal of NLPs administered i.p. was dispersed throughout the kidney and liver and almost no signal was visible after 48 hrs. In contrast, almost the entire fluorescence signal was observed localized in the lung at all time points after i.n. administration. Interestingly, the overall half-live of the NLP after i.p. administration (~15 hr) was longer than what was observed after i.n. administration (~5 hr), even though some NLP signal was evident over a longer time period in the lung than the other tissues after i.n. administration. These findings suggest that

clearance through the lung occurs through a different mechanism after i.n. administration than was observed after i.p. administration. It is worth noting that these experiments were performed by labeling the apoE422k protein and, as such, the data does not necessarily indicate clearance of the intact particle. We are currently evaluating the biodistribution of the intact particle versus the lipid and apoE422k components by fluorescence resonance energy transfer (FRET).

Conclusions

Despite the significant advantages that nanoparticle delivery vehicles have been shown to provide relative to conventional drug delivery systems, numerous limitations need to be addressed to increase the efficacy and broad application of nanoparticulate platforms for delivering therapeutic cargo molecules, including facile functionalization of the platform, *in vivo* stability, targeting specificity, drug entrapment efficiency, long term storage, and toxicity. Here, we evaluated the potential of conjugating a diverse range of biological molecules with disparate chemistries onto the NLP, NLP stability in complex biological fluids, NLP cytotoxicity, and biodistribution after administration through various routes. The amphipathic nature of the NLP platform provided facile conjugation of myriad molecules through either surface conjugation or lipidic anchoring strategies, approaches that can readily be adapted for orthogonal functionalization schemes. Accordingly, we demonstrated successful conjugation of a wide range of different molecules on the NLP, including non-covalent and covalent attachment of proteins as well as incorporation of ssDNA and a small molecule (folate). The NLP was also found to be relatively stable in complex biological fluids, with a half-life as high as 20 hrs in 10% sera and 1 hr in 100% sera. In addition, the NLP platform was nontoxic both *in vitro* and *in vivo*. Finally, the biodistribution of the NLP was found to be highly dependent on the route of administration, where i.n. administration resulted in prolonged retention in the lung tissue and clearance through the kidney and liver was observed after i.p., i.m. and s.c. administration. The combined results of this study suggest that the NLP platform may be ideally suited for use in both passive and targeted in vivo delivery of a wide range of therapeutics molecules.

Acknowledgments

The authors are grateful to Dr. Karl Weisgraber for providing the apoE422k clone and Matt Coleman and Brent Segelke for providing the LcrV clone. This work was performed under the auspices of the U.S. Department of Energy by Lawrence Livermore National Laboratory under Contract DE-AC52-07NA27344 with support from LLNL (LDRD 09-LW-077 awarded to CDB, LDRD 11-LW-015 awarded to NOF, and LDRD 11-ERD-016 awarded to AR). LLNL-JRNL-641712.

References

1. Cho K, Wang X, Nie S, Chen ZG, Shin DM (2008) Therapeutic nanoparticles for drug delivery in cancer. Clin Cancer Res 14: 1310-1316.

2. Mareeva T, Wanjalla C, Schnell MJ, Sykulev Y (2010) A novel composite immunotoxin that suppresses rabies virus production by the infected cells. J Immunol Methods 353: 78-86.

3. Bhatt R, de Vries P, Tulinsky J, Bellamy G, Baker B, et al. (2003) Synthesis and in vivo antitumor activity of poly(l-glutamic acid) conjugates of 20S-camptothecin. J Med Chem 46: 190-193.

4. Kim TY, Kim DW, Chung JY, Shin SG, Kim SC, et al. (2004) Phase I and pharmacokinetic study of Genexol-PM, a cremophor-free, polymeric micelle-formulated paclitaxel, in patients with advanced malignancies. Clin Cancer Res 10: 3708-3716.

5. Malik N, Evagorou EG, Duncan R (1999) Dendrimer-platinate: a novel approach to cancer chemotherapy. Anticancer Drugs 10: 767-776.

6. Markman M (2006) Pegylated liposomal doxorubicin in the treatment of cancers of the breast and ovary. Expert Opin Pharmacother 7: 1469-1474.

7. Manchester M, Singh P (2006) Virus-based nanoparticles (VNPs): platform technologies for diagnostic imaging. Adv Drug Deliv Rev 58: 1505-1522.

8. Wu W, Wieckowski S, Pastorin G, Benincasa M, Klumpp C, et al. (2005) Targeted delivery of amphotericin B to cells by using functionalized carbon nanotubes. Angew Chem Int Ed Engl 44: 6358-6362.

9. Cuenca AG, Jiang H, Hochwald SN, Delano M, Cance WG, et al. (2006) Emerging implications of nanotechnology on cancer diagnostics and therapeutics. Cancer 107: 459-466.

10. Chapman MJ (1980) Animal lipoproteins: chemistry, structure, and comparative aspects. J Lipid Res 21: 789-853.

11. Blanchette CD, Law R, Benner WH, Pesavento JB, Cappuccio JA, et al. (2008) Quantifying size distributions of nanolipoprotein particles with single-particle analysis and molecular dynamic simulations. Journal of Lipid Research 49: 1420-1430.

12. Chromy BA, Arroyo E, Blanchette CD, Bench G, Benner H, et al. (2007) Different apolipoproteins impact nanolipoprotein particle formation. Journal of the American Chemical Society 129: 14348-14354.

13. Fischer NO, Blanchette CD, Segelke BW, Corzett M, Chromy BA, et al. (2010) Isolation, Characterization, and Stability of Discretely-Sized Nanolipoprotein Particles Assembled with Apolipophorin-III. Plos One 5: -.

14. Miyazaki M, Tajima Y, Ishihama Y, Handa T, Nakano M (2013) Effect of phospholipid composition on discoidal HDL formation. Biochim Biophys Acta 1828: 1340-1346.

15. Ma CI, Beckstead JA, Thompson A, Hafiane A, Wang RH, et al. (2012) Tweaking the cholesterol efflux capacity of reconstituted HDL. Biochem Cell Biol 90: 636-645.

16. Toledo JD, Cabaleiro LV, Garda HA, Gonzalez MC (2012) Effect of reconstituted discoidal high-density lipoproteins on lipid mobilization in RAW 264.7 and CHOK1 cells. J Cell Biochem 113: 1208-1216.

17. Hoang A, Drew BG, Low H, Remaley AT, Nestel P, et al. (2012) Mechanism of cholesterol efflux in humans after infusion of reconstituted high-density lipoprotein. Eur Heart J 33: 657-665.

18. Nestler JE, Bamberger M, Rothblat GH, Strauss JF, 3rd (1985) Metabolism of high density lipoproteins reconstituted with [3H]cholesteryl ester and [14C]cholesterol in the rat, with special reference to the ovary. Endocrinology 117: 502-510.

19. Baylon JL, Lenov IL, Sligar SG, Tajkhorshid E (2013) Characterizing the Membrane-Bound State of Cytochrome P450 3A4: Structure, Depth of Insertion, and Orientation. J Am Chem Soc 135: 8542-8551.

20. Justesen BH, Laursen T, Weber G, Fuglsang AT, Moller BL, et al. (2013) Isolation of monodisperse nanodisc-reconstituted membrane proteins using free flow electrophoresis. Anal Chem 85: 3497-3500.

21. Wadsater M, Laursen T, Singha A, Hatzakis NS, Stamou D, et al. (2012) Monitoring shifts in the conformation equilibrium of the membrane protein cytochrome P450 reductase (POR) in nanodiscs. J Biol Chem 287: 34596-34603.

22. Blanchette CD, Cappuccio JA, Kuhn EA, Segelke BW, Benner WH, et al. (2009) Atomic force microscopy differentiates discrete size distributions between membrane protein containing and empty nanolipoprotein particles. Biochim Biophys Acta 1788: 724-731.

23. Cappuccio JA, Blanchette CD, Sulchek TA, Arroyo ES, Kralj JM, et al. (2008) Cell-free co-expression of functional membrane proteins and apolipoprotein, forming soluble nanolipoprotein particles. Mol Cell Proteomics 7: 2246-2253.

24. Cappuccio JA, Hinz AK, Kuhn EA, Fletcher JE, Arroyo ES, et al. (2009) Cell-free expression for nanolipoprotein particles: building a high-throughput membrane protein solubility platform. Methods Mol Biol 498: 273-296.

25. Tufteland M, Ren G, Ryan RO (2008) Nanodisks derived from amphotericin B lipid complex. J Pharm Sci 97: 4425-4432.

26. Yuan Y, Wang W, Wang B, Zhu H, Zhang B, et al. (2013) Delivery of hydrophilic drug doxorubicin hydrochloride-targeted liver using apoAI as carrier. J Drug Target 21: 367-374.

27. Ding Y, Wang W, Feng M, Wang Y, Zhou J, et al. (2012) A biomimetic nanovector-mediated targeted cholesterol-conjugated siRNA delivery for tumor gene therapy. Biomaterials 33: 8893-8905.

28. Gaidukov L, Bar D, Yacobson S, Naftali E, Kaufman O, et al. (2009) In vivo administration of BL-3050: highly stable engineered PON1-HDL complexes. BMC Clin Pharmacol 9: 18.

29. Frias JC, Ma Y, Williams KJ, Fayad ZA, Fisher EA (2006) Properties of a versatile nanoparticle platform contrast agent to image and characterize atherosclerotic plaques by magnetic resonance imaging. Nano Lett 6: 2220-2224.

30. Fischer NO, Infante E, Ishikawa T, Blanchette CD, Bourne N, et al. (2010) Conjugation to nickel-chelating nanolipoprotein particles increases the potency and efficacy of subunit vaccines to prevent West Nile encephalitis. Bioconjug Chem 21: 1018-1022.

31. Fischer NO, Rasley A, Corzett M, Hwang MH, Hoeprich PD, et al. (2013) Colocalized delivery of adjuvant and antigen using nanolipoprotein particles enhances the immune response to recombinant antigens. J Am Chem Soc 135: 2044-2047.

32. Bhattacharya P, Grimme S, Ganesh B, Gopisetty A, Sheng JR, et al. (2010) Nanodisc-incorporated hemagglutinin provides protective immunity against influenza virus infection. J Virol 84: 361-371.

33. Fischer NO, Blanchette CD, Chromy BA, Kuhn EA, Segelke BW, et al. (2009) Immobilization of His-tagged proteins on nickel-chelating nanolipoprotein particles. Bioconjug Chem 20: 460-465.

34. Rensen PC, de Vrueh RL, Kuiper J, Bijsterbosch MK, Biessen EA, et al. (2001) Recombinant lipoproteins: lipoprotein-like lipid particles for drug targeting. Adv Drug Deliv Rev 47: 251-276.

35. Chromy BA, Arroyo E, Blanchette CD, Bench G, Benner H, et al. (2007) Different apolipoproteins impact nanolipoprotein particle formation. J Am Chem Soc 129: 14348-14354.

36. Blanchette CD, Fischer NO, Corzett M, Bench G, Hoeprich PD (2010) Kinetic analysis of his-tagged protein binding to nickel-chelating nanolipoprotein particles. Bioconjug Chem 21: 1321-1330.

37. Fischer NO, Rasley A, Corzett M, Hwang MH, Hoeprich PD, et al. (2013) Colocalized delivery of adjuvant and antigen using nanolipoprotein particles enhances the immune response to recombinant antigens. Journal of the American Chemical Society 135: 2044-2047.

38. Lattuada M, Hatton TA (2007) Functionalization of monodisperse magnetic nanoparticles. Langmuir 23: 2158-2168.

39. Corbierre MK, Cameron NS, Lennox RB (2004) Polymer-stabilized gold nanoparticles with high grafting densities. Langmuir 20: 2867-2873.

40. Jia H, Titmuss S (2009) Polymer-functionalized nanoparticles: from stealth viruses to biocompatible quantum dots. Nanomedicine (Lond) 4: 951-966.

41. Ackermann L, Potukuchi HK, Landsberg D, Vicente R (2008) Copper-catalyzed "click" reaction/direct arylation sequence: modular syntheses of 1,2,3-triazoles. Org Lett 10: 3081-3084.

42. Karver MR, Weissleder R, Hilderbrand SA (2012) Bioorthogonal reaction pairs enable simultaneous, selective, multi-target imaging. Angew Chem Int Ed Engl 51: 920-922.

43. Simon M, Zangemeister-Wittke U, Pluckthun A (2012) Facile double-functionalization of designed ankyrin repeat proteins using click and thiol chemistries. Bioconjug Chem 23: 279-286.

44. Zhang P, Liu S, Gao D, Hu D, Gong P, et al. (2012) Click-Functionalized Compact Quantum Dots Protected by Multidentate-Imidazole Ligands: Conjugation-Ready Nanotags for Living-Virus Labeling and Imaging. Journal of the American Chemical Society.

45. Trang P, Weidhaas JB, Slack FJ (2008) MicroRNAs as potential cancer therapeutics. Oncogene 27 Suppl 2: S52-57.

46. Gref R, Minamitake Y, Peracchia MT, Trubetskoy V, Torchilin V, et al. (1994) Biodegradable long-circulating polymeric nanospheres. Science 263: 1600-1603.

47. Nguyen CA, Allemann E, Schwach G, Doelker E, Gurny R (2003) Cell interaction studies of PLA-MePEG nanoparticles. Int J Pharm 254: 69-72.

48. Lynch I, Cedervall T, Lundqvist M, Cabaleiro-Lago C, Linse S, et al. (2007) The nanoparticle-protein complex as a biological entity; a complex fluids and surface science challenge for the 21st century. Adv Colloid Interface Sci 134-135: 167-174.

49. Salvati A, Pitek AS, Monopoli MP, Prapainop K, Bombelli FB, et al. (2013) Transferrin-functionalized nanoparticles lose their targeting capabilities when a biomolecule corona adsorbs on the surface. Nat Nanotechnol 8: 137-143.

50. Gao T, Blanchette CD, He W, Bourguet F, Ly S, et al. (2011) Characterizing diffusion dynamics of a membrane protein associated with nanolipoproteins using fluorescence correlation spectroscopy. Protein Sci 20: 437-447.

51. Fischer NO, Blanchette CD, Segelke BW, Corzett M, Chromy BA, et al. (2010) Isolation, characterization, and stability of discretely-sized nanolipoprotein particles assembled with apolipophorin-III. PLoS One 5: e11643.

52. Goodman CM, McCusker CD, Yilmaz T, Rotello VM (2004) Toxicity of gold nanoparticles functionalized with cationic and anionic side chains. Bioconjug Chem 15: 897-900.

53. Murphy CJ, Gole AM, Stone JW, Sisco PN, Alkilany AM, et al. (2008) Gold nanoparticles in biology: beyond toxicity to cellular imaging. Acc Chem Res 41: 1721-1730.

54. Chen HT, Neerman MF, Parrish AR, Simanek EE (2004) Cytotoxicity, hemolysis, and acute in vivo toxicity of dendrimers based on melamine, candidate vehicles for drug delivery. Journal of the American Chemical Society 126: 10044-10048.

55. Fotakis G, Timbrell JA (2006) In vitro cytotoxicity assays: comparison of LDH, neutral red, MTT and protein assay in hepatoma cell lines following exposure to cadmium chloride. Toxicol Lett 160: 171-177.

56. Mehrabian M, Castellani LW, Wen PZ, Wong J, Rithaporn T, et al. (2000) Genetic control of HDL levels and composition in an interspecific mouse cross (CAST/Ei x C57BL/6J). J Lipid Res 41: 1936-1946.

57. Ziv O, Avtalion RR, Margel S (2008) Immunogenicity of bioactive magnetic nanoparticles: natural and acquired antibodies. J Biomed Mater Res A 85: 1011-1021.

58. Ochsenbein AF, Zinkernagel RM (2000) Natural antibodies and complement link innate and acquired immunity. Immunol Today 21: 624-630.

59. Irngartinger M, Camuglia V, Damm M, Goede J, Frijlink HW (2004) Pulmonary delivery of therapeutic peptides via dry powder inhalation: effects of micronisation and manufacturing. Eur J Pharm Biopharm 58: 7-14.

60. Courrier HM, Butz N, Vandamme TF (2002) Pulmonary drug delivery systems: recent developments and prospects. Crit Rev Ther Drug Carrier Syst 19: 425-498.

61. Azarmi S, Roa WH, Lobenberg R (2008) Targeted delivery of nanoparticles for the treatment of lung diseases. Adv Drug Deliv Rev 60: 863-875.

62. Niven RW (1995) Delivery of biotherapeutics by inhalation aerosol. Crit Rev Ther Drug Carrier Syst 12: 151-231.

Figure Legends

Figure 1. Schematic of methodologies for conjugating biological or therapeutic molecules to the NLP platform. Conjugation to NLPs can be achieved using A) functional lipids incorporated into the NLP lipid bilayer, B) biomolecules featuring lipidic moieties, or C) combinations of the two.

Figure 2. Conjugation of protein (0841) to the NLP platform. SEC traces of A) NiNLPs incubated with His-tagged 0841 and C) N_3NLPs incubated with DBCO-functionalized 0841 at protein-to-NLP ratios ranging from 0 to 40 and 0 to 160, respectively. The 0841:NLP complexes were purified by SEC, and SDS-PAGE and densitometry were used to quantify 0841 conjugation to B) NiNLPs and D) N_3NLPs. The relative intensity of the 0841 band increased with an increase in the 0841-to-NLP ratio, indicating an increase in the number of proteins/NLP. The concentration of each protein was determined based on densitometry using standards. These concentrations were used to calculate the number of proteins bound per NLP and were plotted as a function of the ratio used in the reaction.

Figure 3. Conjugation of cODN and PEG-folate to the NLP platform. A) SEC traces of the cODN:NLP constructs at varying cODN:NLP ratios. The increase in absorbance at 280 nm and peak shift indicate successful incorporation of cODN. B) Analysis of cODN incorporation into the NLP. Left axis is the cODN:NLP ratio used during assembly and the x-axis is the amount of cODN incorporated into the particle. C) SEC chromatograms of the PF:NLP constructs at increasing PF-to-NLP ratios. D) Analysis of PF incorporation efficiency into the NLP, represented as a function of the PF-to-NLP assembly ratio (y-axis) vs. PF-to-NLP ratio upon assembly and purification (x-axis).

Figure 4. Stability of DMPC:NLPs in 20% serum assessed by SEC over 24 hrs. The peak at t_R 7.8 min corresponds to NLP and the peak at t_R 12.2 min corresponds to the E422k scaffold. Prolonged incubation of DMPC:NLP at 25°C resulted in NLP degradation, evidenced by a decrease in NLP (t_R 7.8 min) and increase in E422k (t_R 11min) peak absorbance intensities. AF647-labeled E422k absorbance was monitored at 600 nm.

Figure 5. Stability of NLPs as a function of lipid content, temperature, time, and serum concentration. Integrated NLP peak area of the SEC chromatograms for A) DOPC:NLPs incubated at 25°C and B) DMPC:NLPs incubated 25°C. C) $t_{1/2}$ of the DOPC:NLPs (blue line) and DMPC:NLPs (red line) incubated 25°C. Integrated area under the NLP peak of the SEC traces for D) DOPC:NLPs incubated 37°C and E) DMPC:NLPs incubated 37°C. F) $t_{1/2}$ of the DOPC:NLPs (blue line) and DMPC:NLPs (red line) incubated at 37°C. AF647-labeled E422k absorbance was monitored at 600 nm.

Figure 6. *In vitro* cytotoxicity of the NLP platform. A) NLP cytotoxicity was measured using the MTT assay with UMR cells at NLP treatment doses ranging from 6 – 50 μg/ml (values are relative to the positive control; lysed cells). Toxicity of the NLPs measured using a LDH release assay with B) J774 cells at NLP treatment doses ranging from 12 – 52 μg/ml, C) Hep G2 cells at NLP treatment doses ranging from 5 – 320 μg/ml, and D) primary murine immune cells at an NLP dose of 25μg/ml. All values in the LDH release studies were normalized to the positive control (lysed cells). Results are shown as mean values from duplicate experiments, with error bars representing standard deviation values.

Figure 7. Effect on mouse body weights upon repeated NLP administration. Weights of A) male and B) female mice receiving daily NLP injections i.n. (30 μl) or i.p. (100 μl) for 14 consecutive days. Control mice received equal volumes of PBS i.p. over the same 14-day time course. Data represent averaged weights from groups of three animals, with standard deviation error bars.

Figure 8. Effect on mouse organ weights upon repeated NLP administration. Weight of organs obtained from mice that had been administration 25 μg of NLP i.n. (30 μl) or i.p. (100 μl) daily for 14 consecutive days (A-D). Control animals received an equal volume of PBS i.p.(100 μl) daily for 14 days (A-D). Normalized organ weights are represented as (organ weight, g) / (body weight, g). Data represent averaged organ weights from groups of three animals, with standard deviation error bars.

Figure 9. Assessment of NLP immunogenicity. Groups of 10 female BALB/c mice were inoculated either i.n. or i.p. with NLP. As a positive control, a group of mice was injected with a known immunogenic recombinant subunit antigen (LcrV) co-administered with adjuvant (CpG). Serum IgG antibody titers against the scaffold protein, E422k (NLP-ip and NLP-in), or LcrV (LcrV+CpG-ip and LcrV+CpG-in) were assessed 4 weeks post-inoculation. Each data point represents the titer values of an individual mouse.

Figure 10. In vivo biodistribution of the NLP. Groups of 3 mice were injected A) i.p., B) i.m., C) s.c. or D) i.n. with AF750 labeled NLPs. 2, 4 and 24 hrs post injection, organs were excised and fluorescence intensity quantified as a function of time and normalized to total organ weight. Data represents the average normalized fluorescence from groups of three animals, with standard error bars.

Figure 11. In depth in vivo NLP biodistribution assessment upon i.p. and i.n. administration. NLP were administered to groups of 2 animals by A) i.p. or B) i.n. routes, and assessed over 72 or 96 hours, respectively. Organ fluorescence was determined *ex vivo* and normalized to total organ weight. The normalized fluorescent intensity was quantitatively measured as a function of time. Data points represent average normalized fluorescence from groups of two animals.

Figure 1

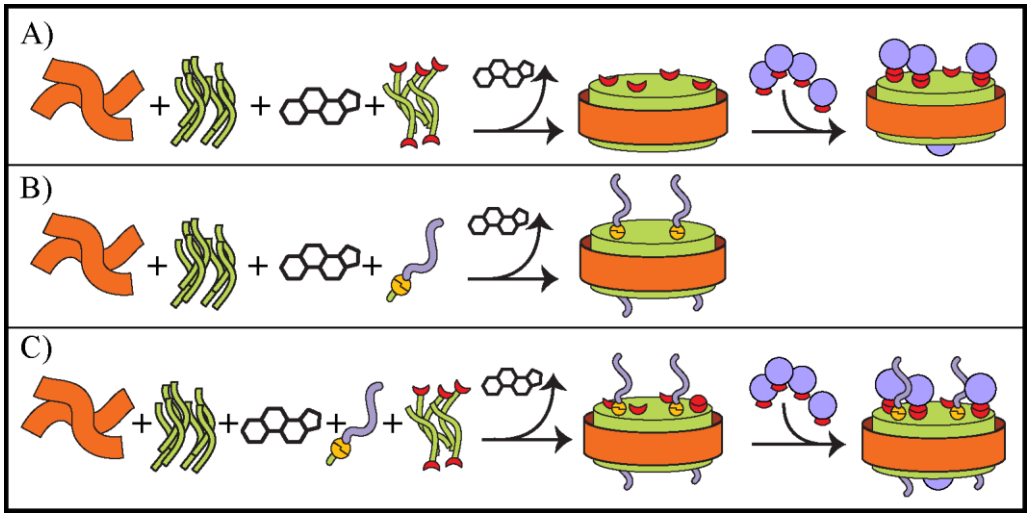

Figure 2

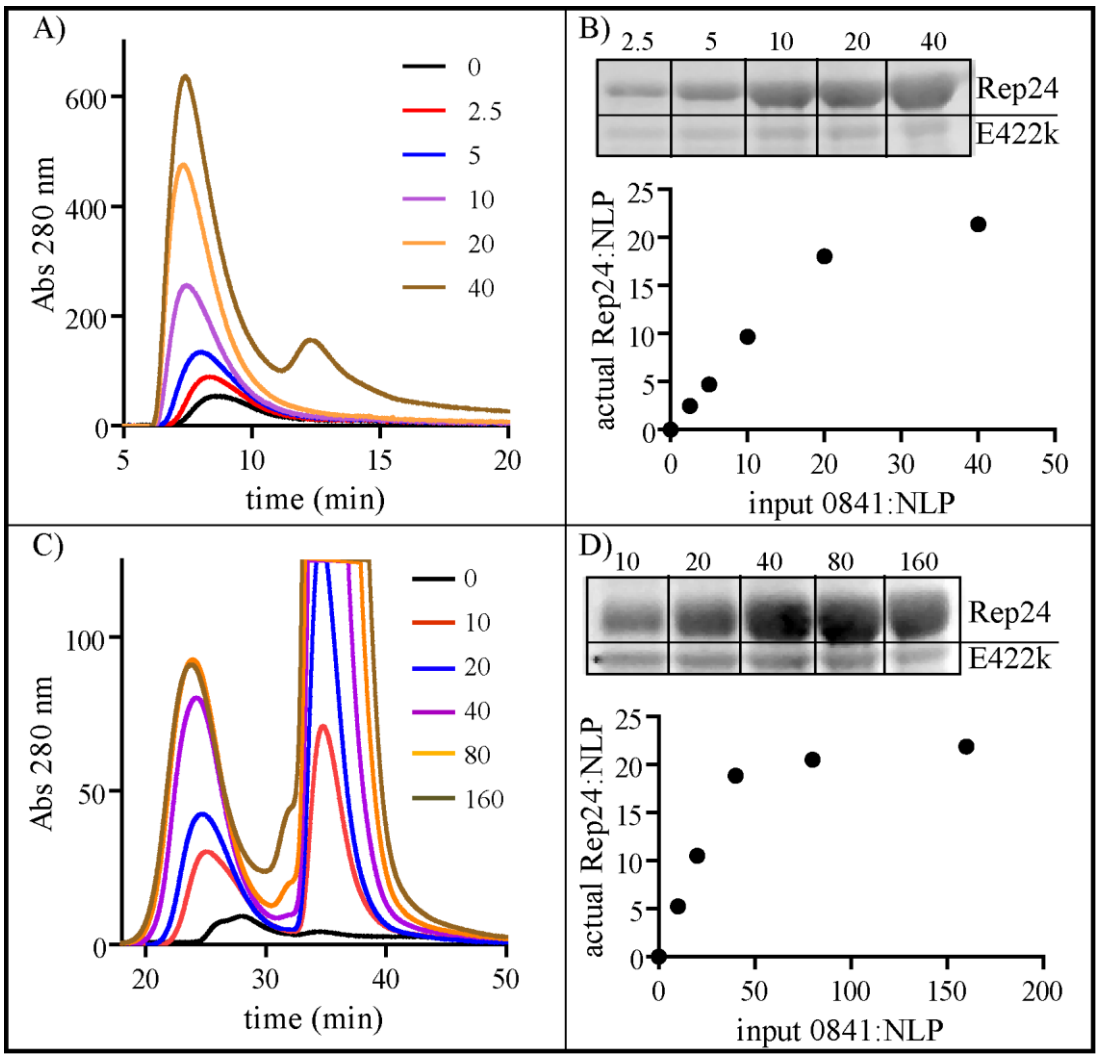
A)
Abs 280 nm
time (min)
0
2.5
5
10
20
40
B)
2.5
5
10
20
40
Rep24
E422k
actual Rep24:NLP
input 0841:NLP
C)
Abs 280 nm
time (min)
0
10
20
40
80
160
D)
10
20
40
80
160
Rep24
E422k
actual Rep24:NLP
input 0841:NLP

Figure 3

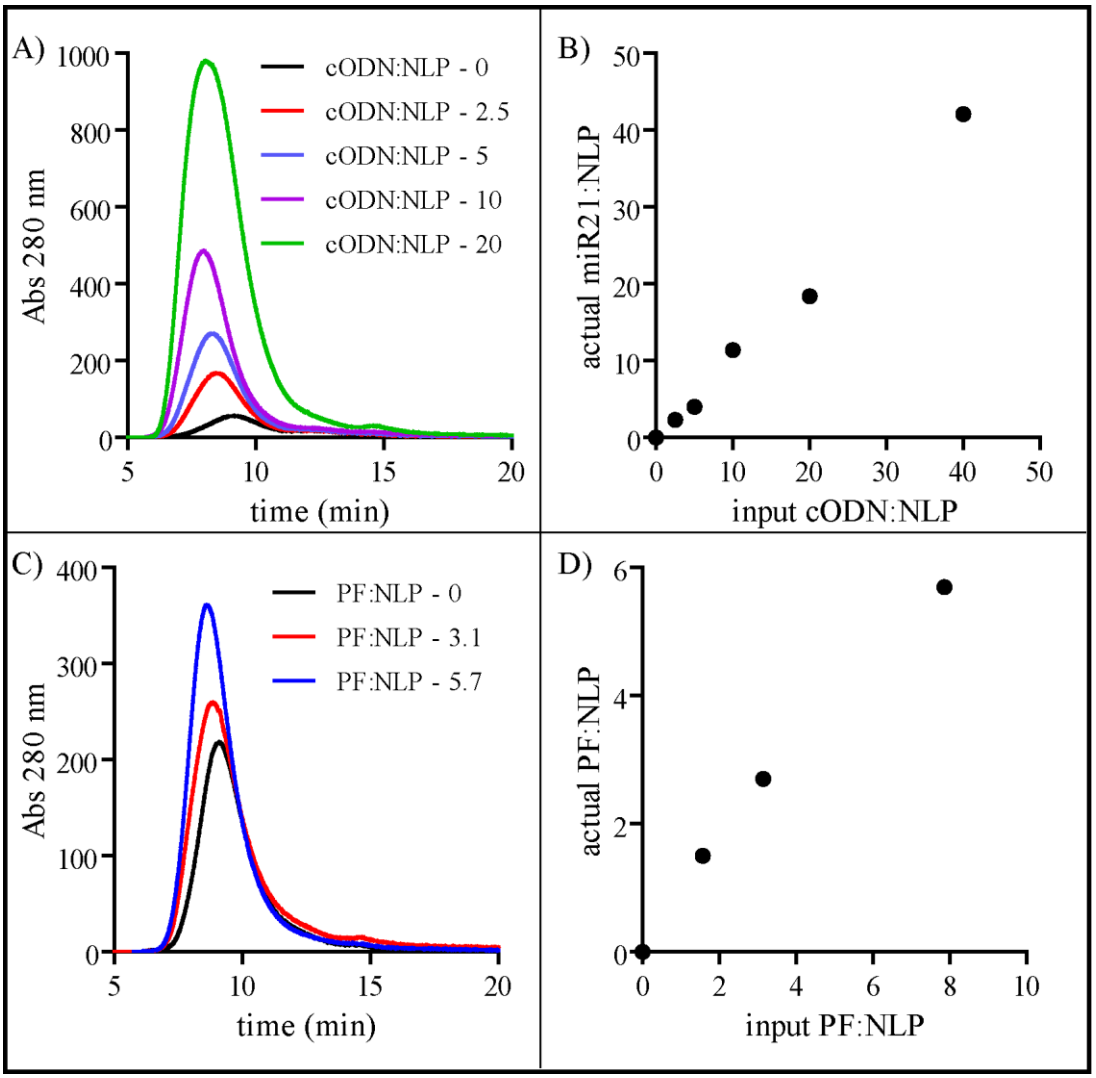
A)
Abs 280 nm
time (min)
cODN:NLP - 0
cODN:NLP - 2.5
cODN:NLP - 5
cODN:NLP - 10
cODN:NLP - 20
B)
actual miR21:NLP
input cODN:NLP
C)
Abs 280 nm
time (min)
PF:NLP - 0
PF:NLP - 3.1
PF:NLP - 5.7
D)
actual PF:NLP
input PF:NLP

Figure 4

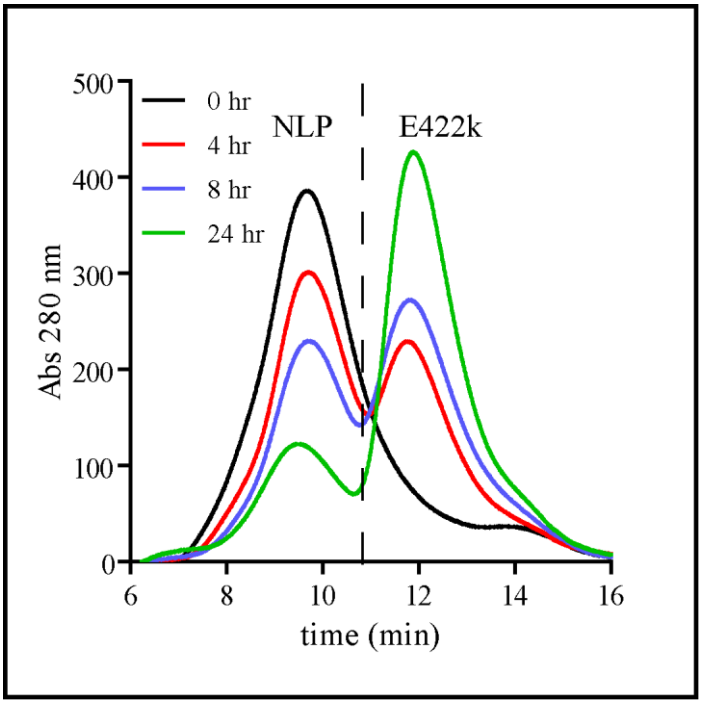
500
400
300
200
100
0
Abs 280 nm
0 hr
4 hr
8 hr
24 hr
NLP
E422k
6
8
10
12
14
16
time (min)

Figure 5

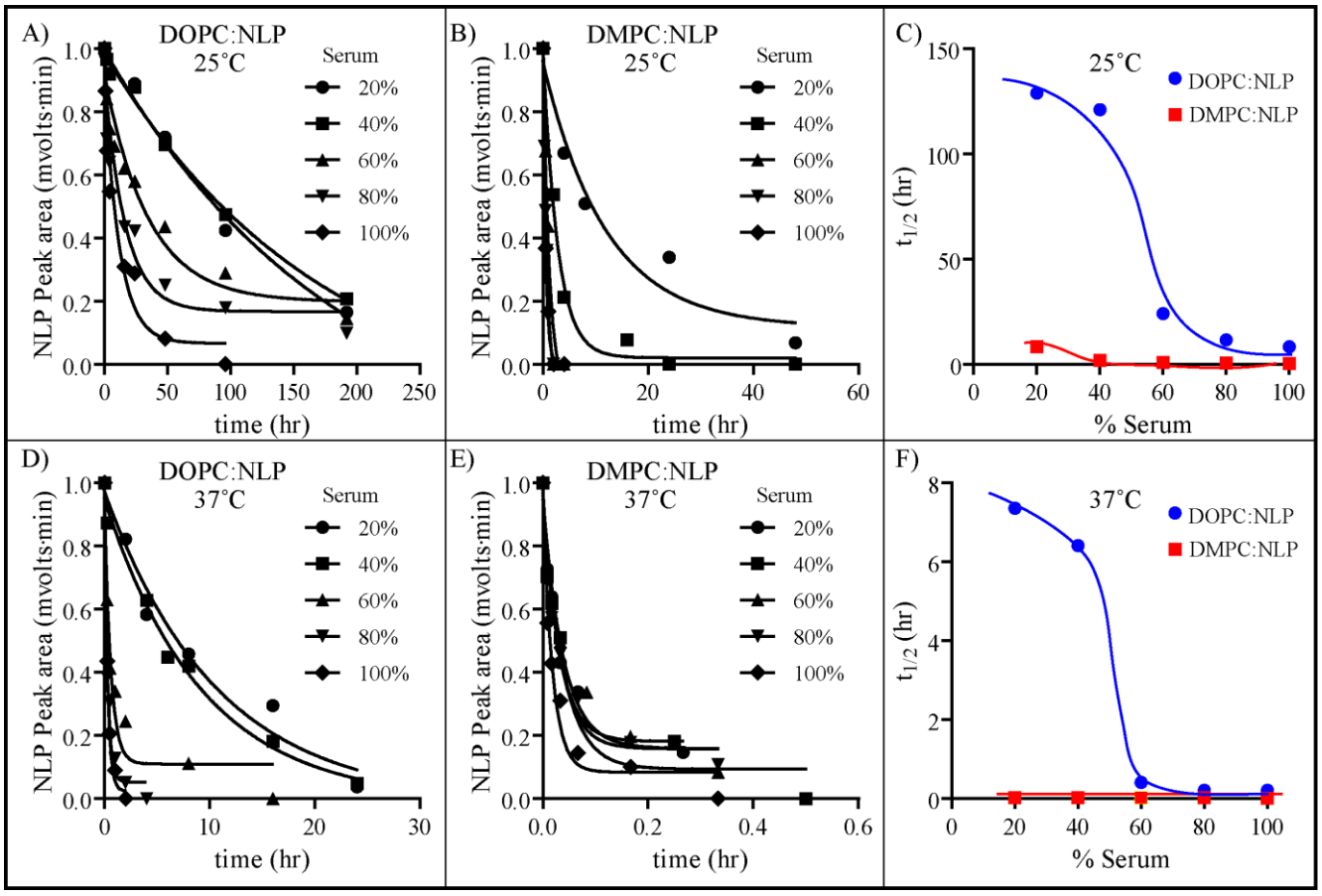
A)
DOPC:NLP
25°C
Serum
20%
40%
60%
80%
100%
NLP Peak area (mvolts·min)
time (hr)
B)
DMPC:NLP
25°C
C)
25°C
DOPC:NLP
DMPC:NLP
$t_{1/2}$ (hr)
% Serum
D)
DOPC:NLP
37°C
E)
DMPC:NLP
37°C
F)
37°C

Figure 6

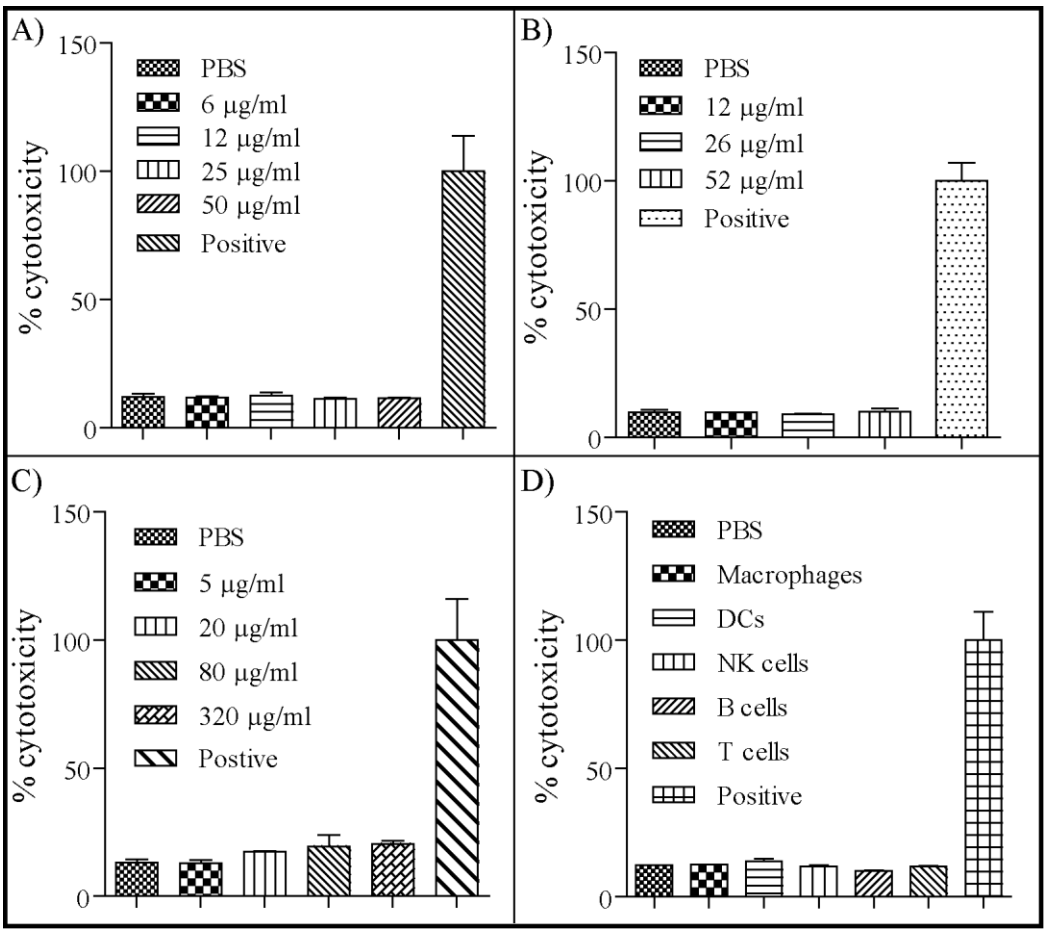
A)
% cytotoxicity
150
100
50
0
PBS
6 µg/ml
12 µg/ml
25 µg/ml
50 µg/ml
Positive
B)
% cytotoxicity
150
100
50
0
PBS
12 µg/ml
26 µg/ml
52 µg/ml
Positive
C)
% cytotoxicity
150
100
50
0
PBS
5 µg/ml
20 µg/ml
80 µg/ml
320 µg/ml
Postive
D)
% cytotoxicity
150
100
50
0
PBS
Macrophages
DCs
NK cells
B cells
T cells
Positive

Figure 7

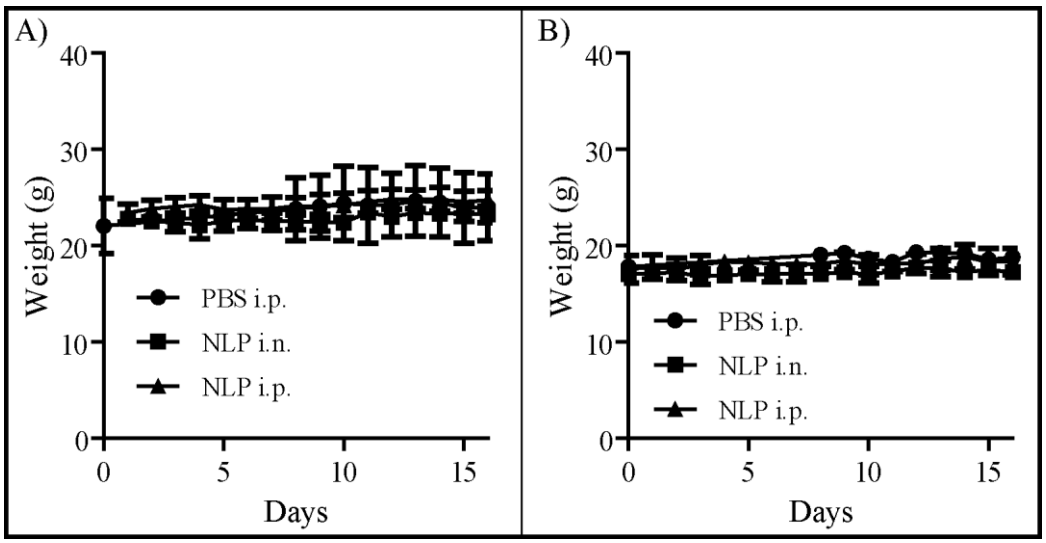
A)
Weight (g)
40
30
20
10
0
0
5
10
15
Days
PBS i.p.
NLP i.n.
NLP i.p.
B)
Weight (g)
40
30
20
10
0
0
5
10
15
Days
PBS i.p.
NLP i.n.
NLP i.p.

Figure 8

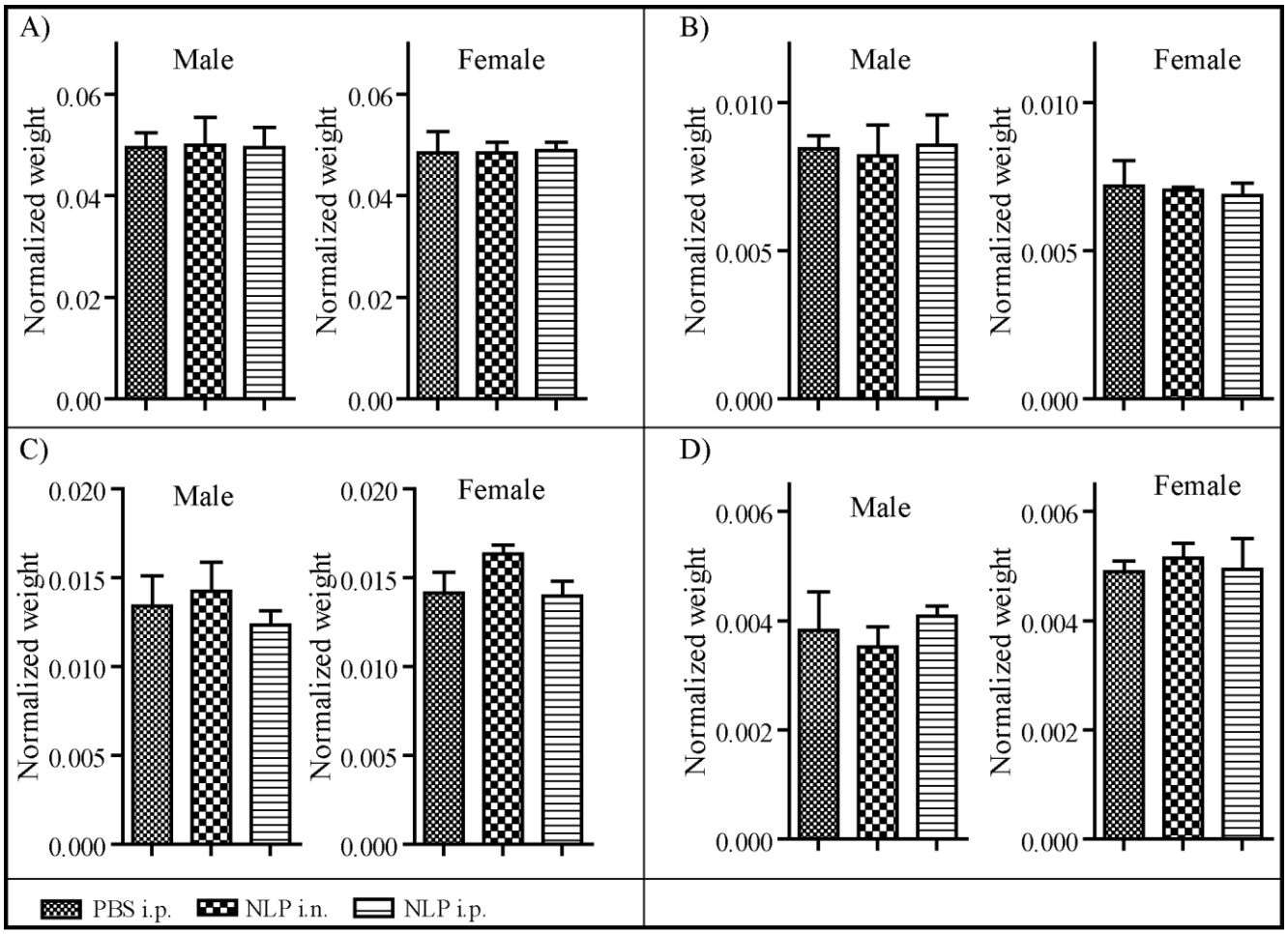
A)
Male
Female
Normalized weight
0.06
0.04
0.02
0.00
B)
Male
Female
Normalized weight
0.010
0.005
0.000
C)
Male
Female
Normalized weight
0.020
0.015
0.010
0.005
0.000
D)
Male
Female
Normalized weight
0.006
0.004
0.002
0.000
PBS i.p.
NLP i.n.
NLP i.p.

Figure 9

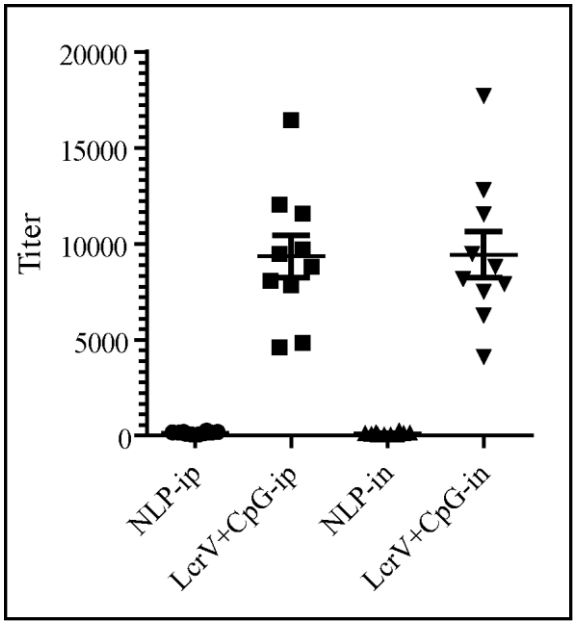
20000
15000
10000
5000
0
Titer
NLP-ip
LcrV+CpG-ip
NLP-in
LcrV+CpG-in

Figure 10

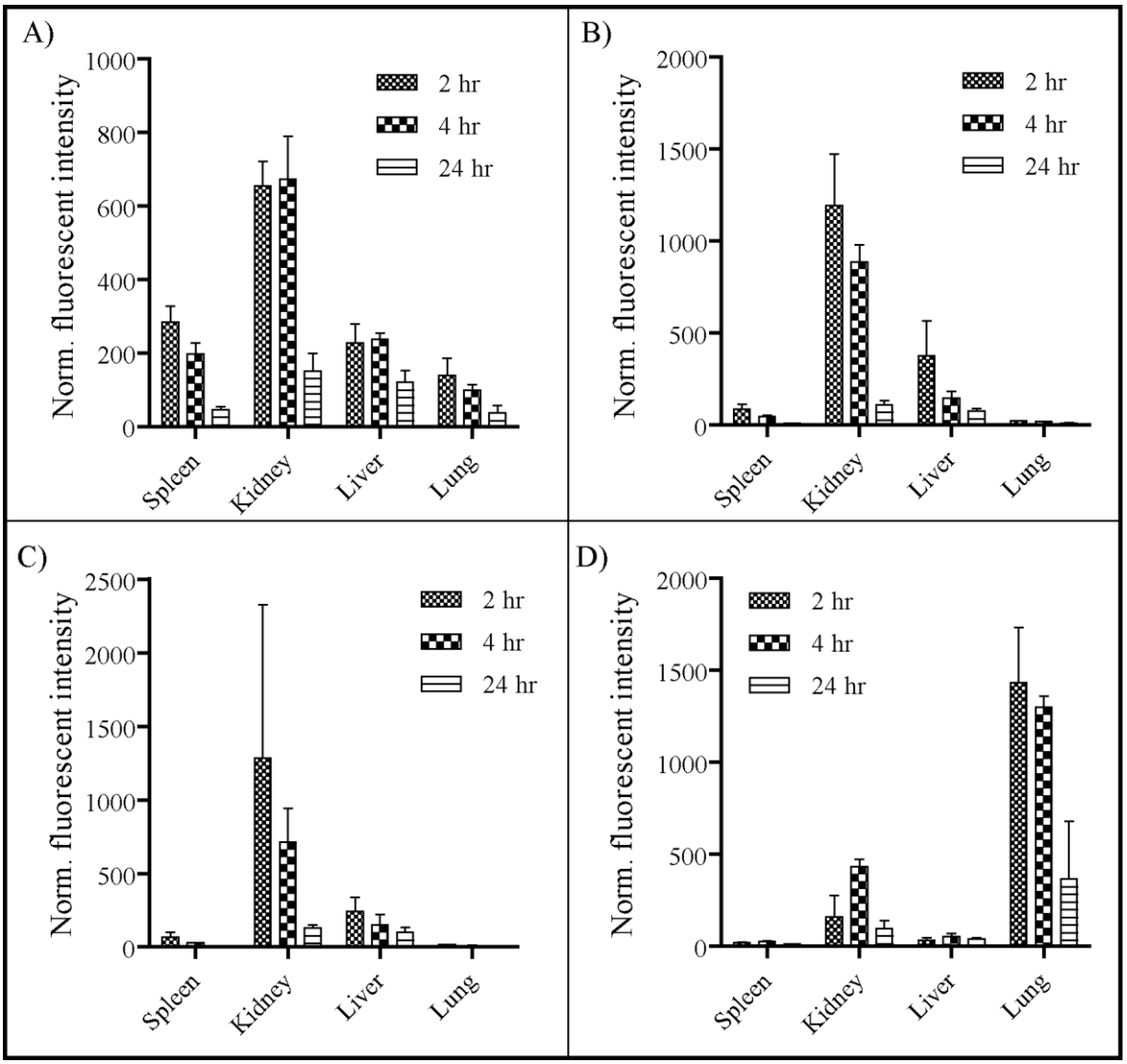
A)
Norm. fluorescent intensity
1000
800
600
400
200
0
2 hr
4 hr
24 hr
Spleen
Kidney
Liver
Lung
B)
Norm. fluorescent intensity
2000
1500
1000
500
0
2 hr
4 hr
24 hr
Spleen
Kidney
Liver
Lung
C)
Norm. fluorescent intensity
2500
2000
1500
1000
500
0
2 hr
4 hr
24 hr
Spleen
Kidney
Liver
Lung
D)
Norm. fluorescent intensity
2000
1500
1000
500
0
2 hr
4 hr
24 hr
Spleen
Kidney
Liver
Lung

Figure 11

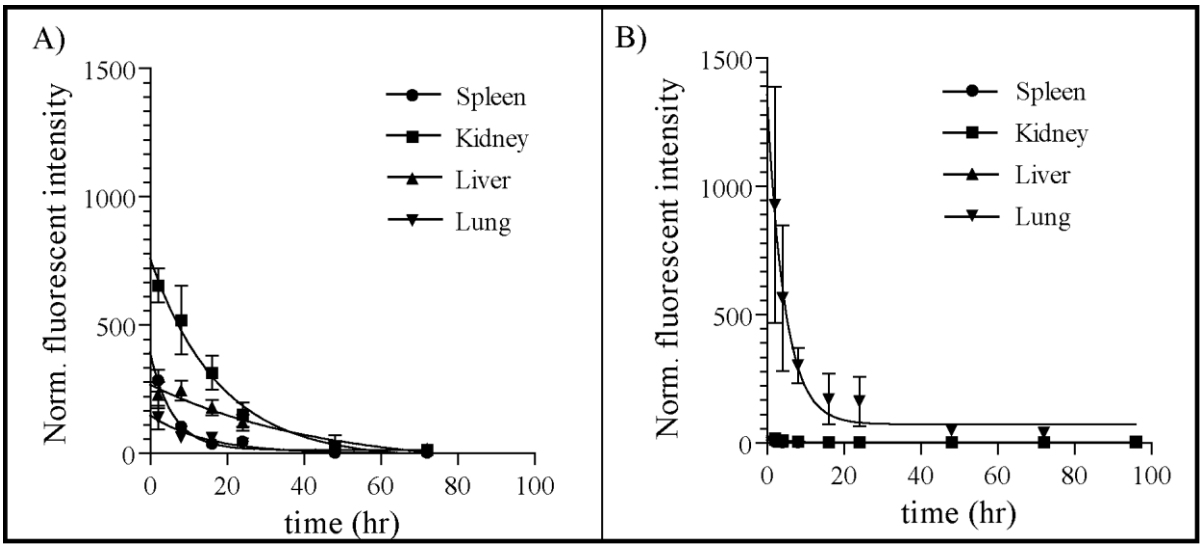
A)
Norm. fluorescent intensity
1500
1000
500
0
0
20
40
60
80
100
time (hr)
Spleen
Kidney
Liver
Lung
B)
Norm. fluorescent intensity
1500
1000
500
0
0
20
40
60
80
100
time (hr)
Spleen
Kidney
Liver
Lung